# We are IntechOpen, the world's leading publisher of Open Access books Built by scientists, for scientists

**4,800**
Open access books available

**122,000**
International authors and editors

**135M**
Downloads

Our authors are among the

**154**
Countries delivered to

**TOP 1%**
most cited scientists

**12.2%**
Contributors from top 500 universities

CLARIVATE ANALYTICS BOOK CITATION INDEX INDEXED

WEB OF SCIENCE™

Selection of our books indexed in the Book Citation Index in Web of Science™ Core Collection (BKCI)

## Interested in publishing with us?
## Contact book.department@intechopen.com

Numbers displayed above are based on latest data collected.
For more information visit www.intechopen.com

Chapter 11

# Detection of Breast Cancer Lumps Using Scattered X-Ray Profiles: A Monte Carlo Simulation Study

Wael M. Elshemey

Additional information is available at the end of the chapter

http://dx.doi.org/10.5772/52787

## 1. Introduction

The difference in the position of the main scattering peak of adipose and soft tissue has been utilized by many authors for the purpose of differentiating between healthy and malignant excised breast tissue samples. Evans et al 1991 [3] measured the x-ray scattering profiles of nineteen samples of healthy and diseased human breast tissues. They reported that while large differences were found in the shapes of scattered photon distributions between adipose and fibroglandular tissues, only small differences existed between carcinomas and fibroglandular tissue.

Kidane et al 1999 [2] measured the diffraction patterns of one hundred excised breast tissue samples. They found that breast tissue types could be characterized on the basis of the shape of scattered spectrum (from 1.0 to 1.8$nm^{-1}$) and the relative intensities of the adipose and fat free peaks at 1.1 and 1.6$nm^{-1}$ respectively.

Poletti et al 2002a [4] found that the scattered photon distribution of healthy and cancerous breast tissues were considerably different. They also found differences in the scattered photon distributions of human breast tissue & breast equivalent materials. They pointed out that the scattered photon distribution of adipose tissue was similar to corresponding commercial breast-equivalent materials and that of glandular tissue was equivalent to water.

Using x-ray from a synchrotron, Ryan and Farquharson 2004 [5 ] showed the well documented differences between the scattering profiles of adipose and diseased (malignant) tissue while Castro et al 2004 [6] measured scattering distributions at six different sites in breast tissue sample and showed that the fat content decreased as the tumor infiltrated the tissue.

Geraki et al 2004 [7] presented averaged diffraction spectra of one hundred and twenty specimens of healthy and tumor breast tissue samples measured using Energy Dispersive X-ray Diffraction (EDXRD) system. Their averaged profiles clearly showed the characteristic diffraction peaks of adipose and fibrous tissues.

Ryan and Farquharson 2007 [8] presented averaged and smoothed x-ray scattering profiles of five different breast tissue classifications measured using an EDXRD system which also measured Compton scattering in order to provide additional information about the electron density of samples. The collected information was utilized by a proposed model that was capable to differentiate between malignant and non-malignant breast tissue samples.

Theodorakou and Farquharson 2008 [9] summarized a collection of contributions by different authors about the application of x-ray diffraction to breast tissue characterization.

Elshemey and Elsharkawy 2009 [10] presented a Monte Carlo simulation code capable of simulating x-ray scattering profiles from breast tissue samples, where breast tissue was considered as a mixture of two main components (e.g. adipose and glandular or adipose and cancer tissues). The Monte Carlo code inputs which resulted in the best fitted simulated profile to a measured profile of an excised breast tissue sample were used to identify and estimate the percentages of the two main breast tissue components in the measured sample.

Bohndiek et al 2009 [11] used an active pixel sensor x-ray diffraction (APXRD) system in order to measure scatter profiles from biopsy-equivalent samples of different compositions (from 100% fat to 100% fibrous tissue). The measured profiles were used to build a model that was capable of accurately predicting the fat content of a series of unknown samples.

Elshemey et al 2010 [12] evaluated the diagnostic capability of x-ray scattering parameters (the full width at half maximum FWHM and area under the x-ray scattering profile of breast tissue in addition to the ratio of scattering intensities $I_2$ / $I_1$% at 1.6 $nm^{-1}$ to that at 1.1 $nm^{-1}$ corresponding to scattering from soft and adipose tissues, respectively) for the characterization of breast cancer. They reported high sensitivity, specificity and diagnostic accuracy of the examined parameters for the probing of breast cancer in excised tissue samples.

In spite of the wide research work aiming to differentiate between healthy and malignant breast tissues in excised samples using the pronounced differences in their x-ray scattering profiles, yet performing a research work to investigate the applicability of this technique for the detection of breast cancer in a whole breast of a patient would probably face many difficulties: First, the data obtained from the small-sized excised breast tissue samples do not account for multiple scattering effects which would probably affect the shape of scattered photon distribution in case of whole breast of normal dimension. Second, it is not acceptable (for many known reasons) to perform test measurements directly on patients. Even if this were possible, still there will be a great difficulty in correlating the measured profiles to a specific histopathology in breast tissue. Third, an alternative approach may be performing research on breast phantoms. Unfortunately, the available breast phantom materials are only excellent in mimicking the attenuation properties of breast tissue rather than producing an x-ray scattered photon distribution equivalent to scattering from breast tissue [4]. More-

http://dx.doi.org/10.5772/52787

over, what would be the tissue-equivalent material that produces a scattered photon distribution similar to breast cancer?

For these reasons, the present work introduces Monte Carlo simulation of photon transport inside a model breast in the presence and in the absence of breast cancer lump as a suggested means to examine the possibility of characterizing breast cancer in patient breast using the angular distribution of scattered x-ray photons.

## 2. Theoretical background

At the energy range (15 to 40 keV) encountered in mammography [13, 14], an incident x-ray photon will interact with breast tissue either by photoelectric absorption, Compton (inelastic, incoherent) scattering or Rayleigh (elastic, coherent) scattering.

If photoelectric absorption takes place, the incident photon energy will be absorbed by bound atomic electrons leading to the removal of such photons from the incident beam. The attenuation of an x-ray beam in mammography is due to all three interaction processes.

For a biological sample of known composition, its mass attenuation coefficient $\mu/\rho$ can be approximately evaluated from the tabulated coefficients $\mu_i / \rho_i$ for the constituent elements according to the weighted average $w_i$ of each element, where:

$$\frac{\mu}{\rho} = \sum_i \frac{w_i \mu_i}{\rho_i} \quad or \quad \mu = \rho . \sum_i \frac{w_i \mu_i}{\rho_i} \tag{1}$$

$\mu_i$ and $\rho_i$ are respectively, the attenuation coefficient and density of element $i$, while $\mu$ and $\rho$ are respectively, the linear attenuation coefficient and density of the biological sample [15].

If Compton scattering takes place, the incident photons will impart some of their energy to a loosely bound electron which then leaves the atom while incident photons will be deflected from its initial direction by a scattering angle $\theta$. At low photon energies, incoherent scattering shows small angular variations compared to coherent scattering and as such it would not affect the characterization of tissues based on the angular distribution of coherently scattered photons [1].

The differential cross section of incoherent scattering including electron binding effects can be given as the product of Klein–Nishina differential cross section $d\sigma_{KN,e}/d\Omega$ (for Compton collision between a photon and a free electron) and the incoherent scattering function of an atom $S(x, Z)$ where $x = \sin(\theta/2)/\lambda$ is the momentum transfer variable, $Z$ is the atomic number and $\lambda$ is the wave length of incident photon. $S(x, Z)$ represents the probability that an atom will be raised to any excited or ionized state when a photon imparts a recoil momentum to an atomic electron. The differential cross section of a molecule for incoherent scattering determines the new direction of photon after incoherent scattering and can be written as:

$$\frac{d\sigma_{incoh,m}}{d\Omega} = \frac{d\sigma_{KN,e}}{d\Omega} S_m(x) = \frac{r_o^2}{2}\left(\frac{E'}{E}\right)^2 \left(\frac{E'}{E} + \frac{E}{E'} + \cos^2\theta - 1\right) S_m(x) \tag{2}$$

Where $S_m(x)$ is the incoherent scattering function of a molecule; considering that atomic cross sections for incoherent scattering combine independently. $E$ & $E'$ are the energies of incident and scattered photons, respectively [10].

If Coherent scattering takes place, an incident photon will interact with bound atomic electrons where the struck electron is neither ionized nor excited as there is no energy transfer from the incident photon to the electron. The scattered photon attains a new direction with no loss of energy [9]. Coherent scattering is dominant over incoherent scattering at the energy range of mammography.

The differential coherent scattering cross-section per atom for unpolarized radiation determines the new direction of photon after coherent scattering and can be expressed approximately as:

$$\frac{d_a\sigma_{coh}}{d\Omega} = \frac{r_o^2}{2}\left(1 + \cos^2\theta\right).\left[F(x,Z)\right]^2 \tag{3}$$

Where; $r_o$ is the classical electron radius, θ is the photon scattering angle and,

$$\frac{r_o^2}{2}\left(1 + \cos^2\theta\right) \tag{4}$$

is the energy independent Thomson differential cross-section per electron, ($d_e\sigma_T$ / dΩ). The variable $F(x, Z)$ is called the atomic form factor which is the sum of electronic form factors and represents the ratio of the amplitude of the coherently scattered radiation by an entire atom to that by a single free electron. The square of this form factor is the probability that Z electrons of the atom take up a recoil momentum, ($q$), without absorbing any energy. Similar to the incoherent scattering function of an atom $S(x, Z)$, the atomic form factor $F(x, Z)$ also depends on the momentum transfer variable ($x$), defined before in this section [16].

When considering a molecule, the molecular coherent differential scattering cross-section can be utilized to calculate the scattered photons distribution and is given by:

$$\frac{d_m\sigma_{coh}}{d\Omega} = \frac{r_o^2}{2}\left(1 + \cos^2\theta\right).F_m^2(x) \tag{5}$$

Where $F_m^2(x)$is the square of molecular form factor.

http://dx.doi.org/10.5772/52787

Due to the interference of photons after coherent scattering, the molecular form factors calculated using the independent atomic model employing the sum rule [17] are considerably different from the measured molecular form factors at low values of momentum transfer. Several authors have presented measured molecular form factors for a wide variety of biological tissues (17, 18, 19, 16, 20, 21).

The present work aims at examining the validity of characterizing breast cancer lumps in a breast model. This is based on the idea that the presence of a lump would result in an increase in the amplitude of the x-ray scattering peak due to soft tissue at 1.6 $nm^{-1}$ relative to the breast adipose peak at 1.1 $nm^{-1}$. Moreover, it is expected that an increase in the size of the lump would result in more photons interacting with the lump and consequently an increase in the amplitude of the scattering peak at 1.6$nm^{-1}$ relative to the 1.1 $nm^{-1}$ peak. A linear dependence of the ratio of amplitudes of these two peaks on lump size would be considered a proper evidence of the validity of the suggested method.

A main challenge which faces the ability to characterize a breast lump in a normal breast using the proposed method would probably be the multiple scattering effects. Photons carrying more than one scattering event inside the breast would affect the expected angular distribution of photons exiting the breast. Fortunately, multiple scattering at mammographic energies is considerably low. Chan & Doi 1986 [22] showed that the mean number of interactions for an incident photon inside a water phantom strongly depended on incident photon energy and phantom thickness. They reported a mean number of interactions of 1.2 for photon energy of 15keV incident on a phantom of thickness 5cm in the direction of the beam. These conditions are comparable to those investigated in the present work. For a 20 cm phantom and 100 keV incident photon energy, Chan & Doi 1986 [22] reported a mean number of interactions equal to a maximum of 5.

## 3. Monte Carlo simulation

The present Monte Carlo simulation is a modification of older versions of the Monte Carlo simulations by Elshemey et al 1999 [23] and Elshemey and Elsharkawy 2009 [10]. All three versions represent a step by step tracing of the sampling procedures described in detail by Chan and Doi 1983 [24] with modifications in the algorithm in order to reach different simulation goals. Figure 1 shows a block diagram illustrating the main steps of the simulation algorithm used in this study.

The proposed setup includes a pencil beam of highly collimated monoenergetic photons of known energy (either 20 or 40keV) from a stationary source is allowed to fall on the center of a rectangular uncompressed model breast of fixed average dimension; a thickness of 6cm in the direction of the beam, a width of 18cm and a breadth of 8cm [25, 26]. A cubic model breast cancer lump centered in the direction of the beam may be also present. The size of the lump is selectable ranging from 0.1 up to $3cm^3$, while the depth is either 2 or 4cm below the surface of breast. Similar to the work of Bohndiek et al 2008 [11] and Elshemey & Elsharkawy 2009 [10], pork muscle data is used to simulate breast cancer lump tissue [19, 27]. The

attenuation coefficients for breast tissue and pork muscle are calculated using the sum rule from their elemental composition as shown in the theoretical background section. This work uses the elemental composition of breast tissue used by Peplow and Verghese 1998 [19] in the calculation of their tabulated molecular form factors (H 0.115, C 0.387 and O 0.498) with a breast tissue density of 0.960 g/cm$^3$. The elemental composition of pork muscle is obtained from Kosanetzky et al 1987 [1], (H 0.1, C 0.107, N 0.0275, O 0.75, Cl 7.8 x $10^{-4}$) with a density of 1.066 g/cm$^3$. The data for Cl is not included in the calculation of the attenuation coefficient of pork muscle as its proportion is extremely low.

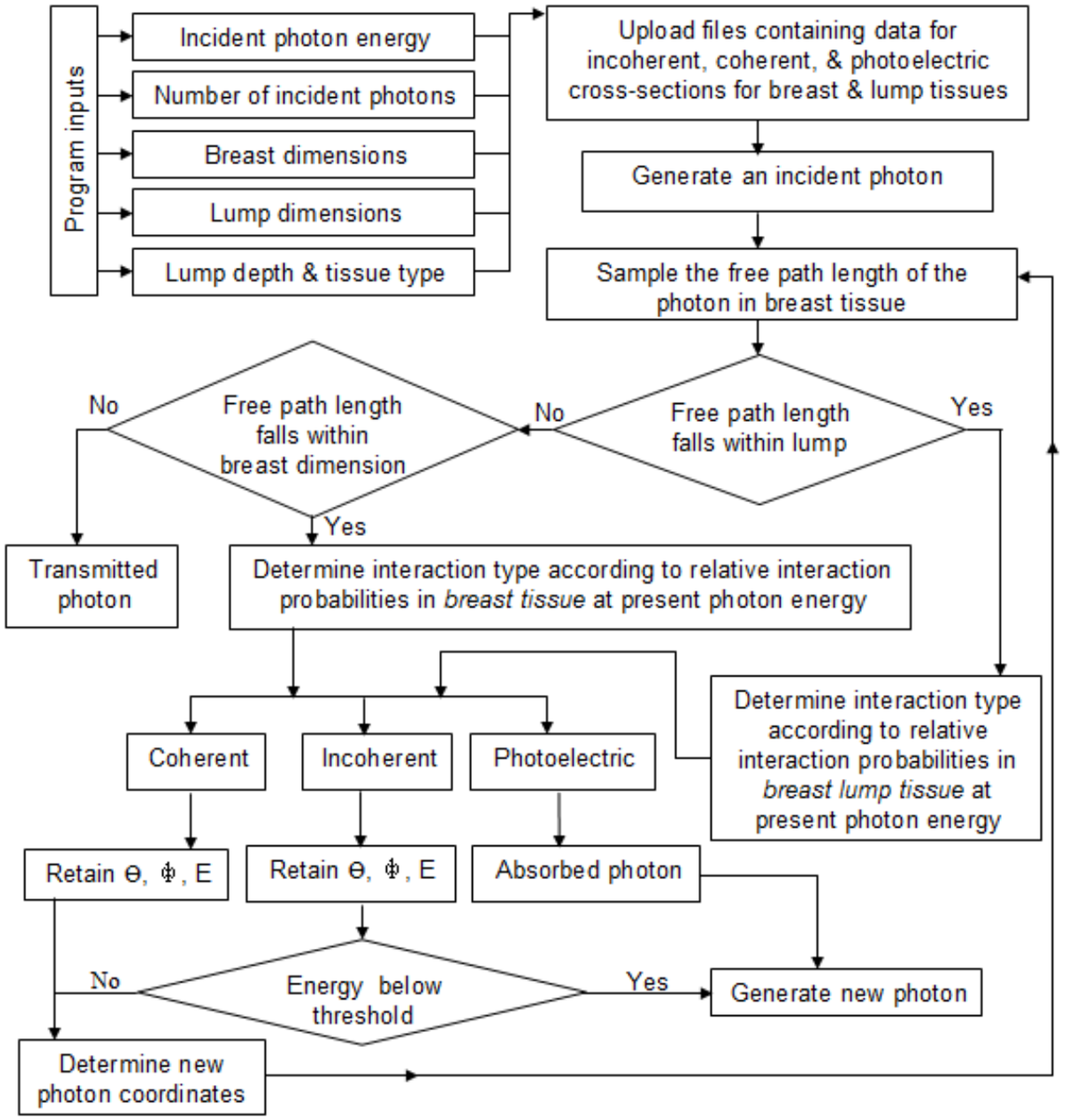


**Figure 1.** Block diagram of the present Monte Carlo simulation steps.

http://dx.doi.org/10.5772/52787

The proposed detector is probably a highly collimated Hyper-pure Germanium or NaI(Th) detector of maximum possible energy resolution and sensitivity. The detector would be able to scan the breast phantom from the direction opposite to the source with high precision.

For each incident photon, the first step is to calculate its free path $t$ in order to predict the first interaction site. This is carried out by sampling from the exponential probability density function: $p(t) = \mu e^{-\mu t}$, such that $t = 1/(\mu \ln r)$, where $r$ is a random number uniformly distributed in the interval [0, 1] and $\mu$ is the total linear attenuation coefficient of breast tissue at the energy of incident photon [24].

If the interaction site falls within the dimension of the lump, then the interaction mechanism of photon in the lump is determined from the relative probabilities of interaction at the given photon energy. A random number is drawn, and according to its value an interaction mechanism is selected [24].

The photon is either absorbed (photoelectric effect) and consequently the program will generate a new photon, or it will be coherently scattered thus the program will continue tracing the photon by calculating the new photon coordinates, new free path length and interaction site taking into consideration the photon scattering angle $(\theta)$ and simulated azimuthal angle $(\phi)$. If the photon is incoherently scattered, the program will follow the same steps as coherent scattering except that it will take into consideration the change in scattered photon energy.

If the new interaction site falls outside the lump and inside the dimension of the breast, the type of interaction will be determined in a way similar to the case of breast lump but in this case using the photon interaction probabilities in breast tissue at the energy of interacting photon. The new photon coordinates; new free path length and interaction site will be determined and so on.

If the free path length of photon at any step falls outside the dimensions of the breast, all photon information including energy and scattering angle will be saved in a file for the development of the x-ray photon scattering profile. All forward scattered photons exiting from the model breast at an angle between $0^0$ (i.e. in the direction of the incident beam) up to $90^0$ are recorded. The data are binned into angles with an increment of $0.5^0$.The program will keep on generating photons up to a pre-defined maximum number of photons. A single run takes only few minutes.

In the present simulation $9 \times 10^6$ photons are generated in each run of the program. For each simulated condition, the code is run three times in order to calculate the standard error in parameters calculated from the scattered photon distribution. Values of incoherent scattering function are obtained from Hubbell et al 1975 [28] and values of measured coherent scattering form factors accounting for molecular interference effects are obtained from Peplow and Verghese 1998 [19], where as values of photon attenuation coefficients are obtained from Hubbell 1977 [29].

## 4. Results and discussion

Figure 2 (a & b) presents simulated x-ray scattering profiles from model breast in the presence and in the absence of a breast cancer lump of different sizes at a depth of 2cm for incident photon energies of 20keV (figure 2a) and 40keV (figure 2b) respectively. For both energies, there is an apparent decrease in the total number of scattered photons with increase in breast lump size. The scattered photon distributions in case of 20keV photons looked noisy where it is hard to resolve the x-ray scattering profiles in the presence of breast lumps of small size variations. This would be attributed to the fact that 20keV photons suffer more attenuation than 40keV photons, where as for the same number of incident photons $9 \times 10^6$, the scattered count in case of 20keV photons is about one order of magnitude less than the case of 40keV photons. On the other hand, the scattered photon distributions of 40keV photons are smooth and even small differences in lump size result in distinguishable differences in the scattering profiles. The adipose peak at $1.1nm^{-1}$ and the soft tissue peak at $1.6nm^{-1}$ are well represented in the scattering profiles of 40keV photons compared to a noisy appearance in case of 20keV photons.

The simulated x-ray scattering profiles from model breast in the presence and in the absence of a breast cancer lump of different sizes at a depth of 4cm for incident photon energies of 20 and 40keV are presented in figure 3 (a & b) respectively. The maximum chosen lump size for breast lumps located at a depth of 4cm is $2cm^3$ because otherwise the tumor will exceed the maximum dimension of the breast in the direction of the incident beam (6 cm). In other words, the tumor will be budding outside the selected model breast dimensions. Almost all of the comments on the x-ray scattering distributions in case of breast lumps located at 2cm still apply on the scattering profiles in case of breast lumps located at 4cm below the surface of breast. The 40keV photons produce scattering profiles which are smoother and more informative than 20keV photons.

In order to test the validity of characterization of cancer lumps inside a breast of normal dimensions using the differences in relative scattered photon intensities at 1.6 to $1.1nm^{-1}$ ($P_2/P_1$%), a plot of $P_2/P_1$% versus lump size is presented in figure 4a for 20 keV incident photons and lump depth of 2cm ($P_2/P_1$% on the right hand axis, data represented by unfilled circles). The graph show a weak linear relationship ($R^2 = 0.6176$) in addition to a small slope reflecting a poor dependence of the $P_2/P_1$% parameter on breast lump size in the model breast. The same poor dependence was also reported for other investigated lump depths and photon energies and as such they are not presented in the other three graphs (b, c & d) in figure 4. One would expect that multiple scattering is the main reason for the ratio $P_2/P_1$% to produce weak correlation towards breast cancer lump size in case of model breast. Multiple scattering may cause a shift in the adipose or soft tissue peak positions which will directly affect the value of the $P_2/P_1$% ratio.

http://dx.doi.org/10.5772/52787

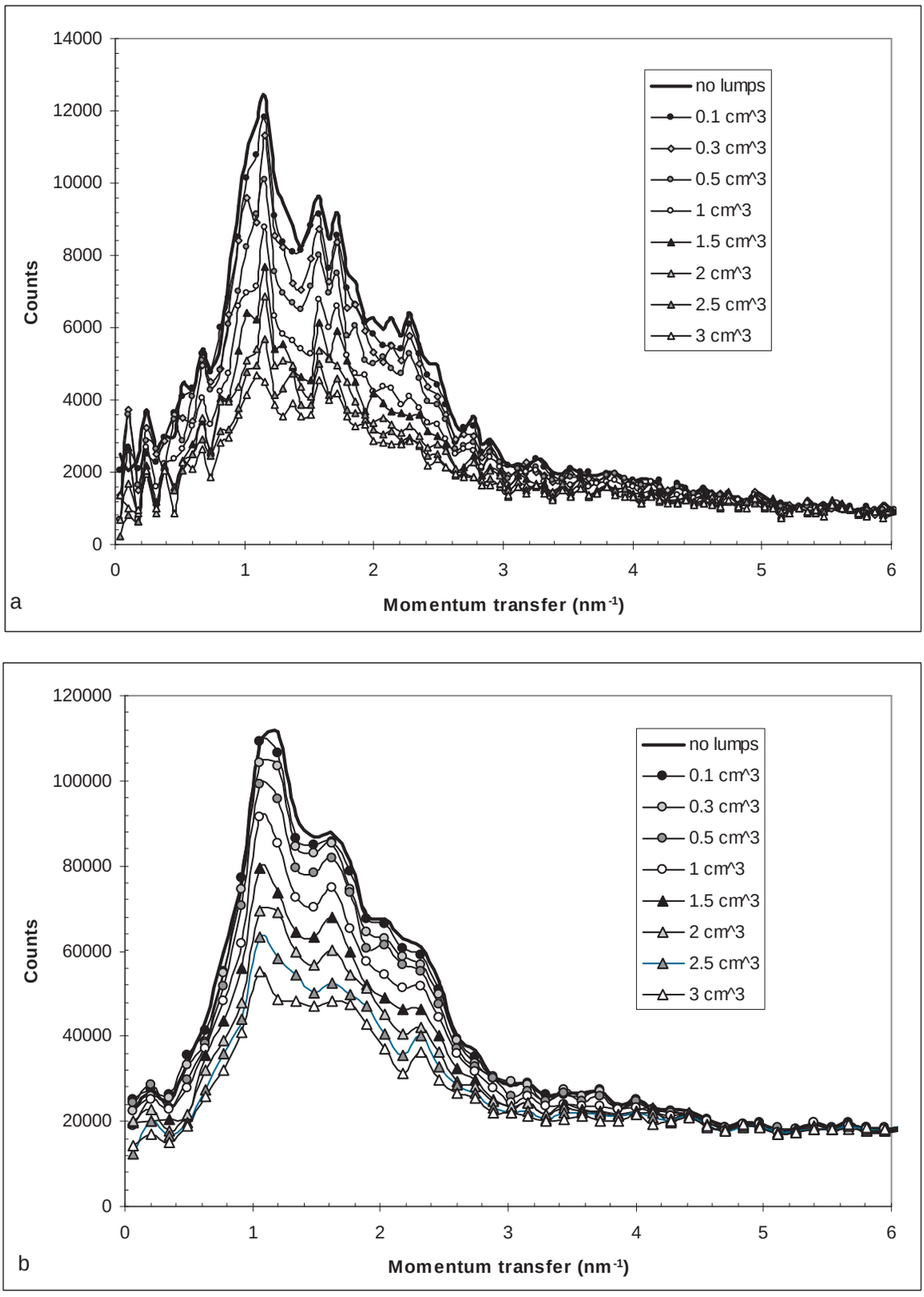


**Figure 2.** X-ray scattering from a model breast containing a breast cancer lump of different sizes at a depth of 2cm and incident photon energies of (a) 20keV and (b) 40keV.

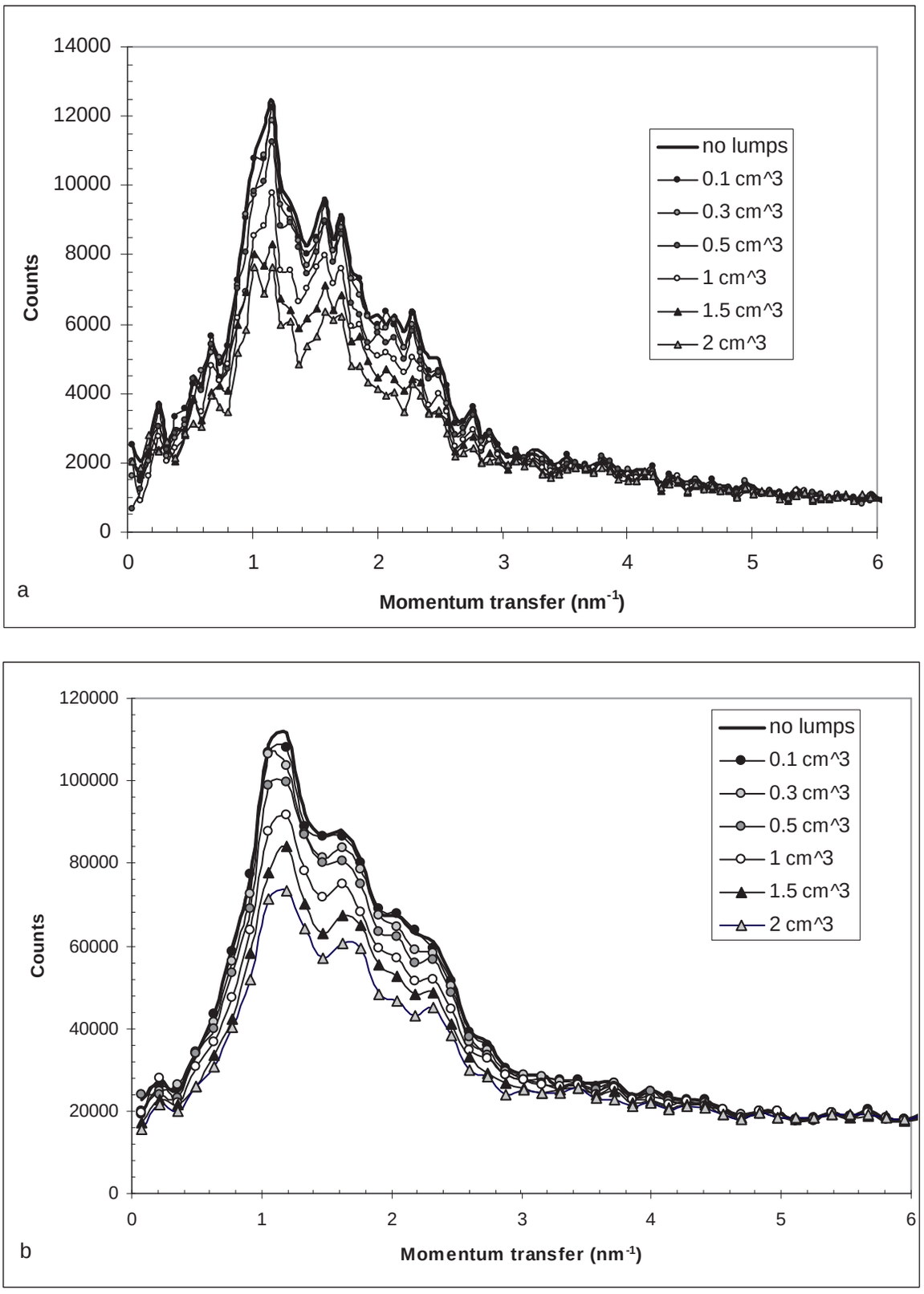


**Figure 3.** X-ray scattering from a model breast containing a breast cancer lump of different sizes at a depth of 4cm and incident photon energies of (a) 20keV and (b) 40keV.

http://dx.doi.org/10.5772/52787

Nevertheless, a plot of the area under the 1.6nm$^{-1}$ peak relative to the area under the 1.1nm$^{-1}$ peak ($A_2/A_1$%) versus lump size yielded much better data linearity ($R^2$ = 0.9684) and a sharp slope (figure 4a) reflecting a degree of dependence of this parameter on breast lump size variations for lumps located at 2cm and incident photon energy of 20keV. The area under the 1.1nm$^{-1}$ peak is determined as the region starting from minimum momentum transfer value up to a momentum transfer value of 1.4nm$^{-1}$, which corresponds to the trough of the valley between the two peaks. The area under the 1.6nm$^{-1}$ peak is calculated as the region starting from the trough up to a momentum transfer value of 5nm$^{-1}$, where the halo due to molecular interference of coherently scattered photons apparently ends.

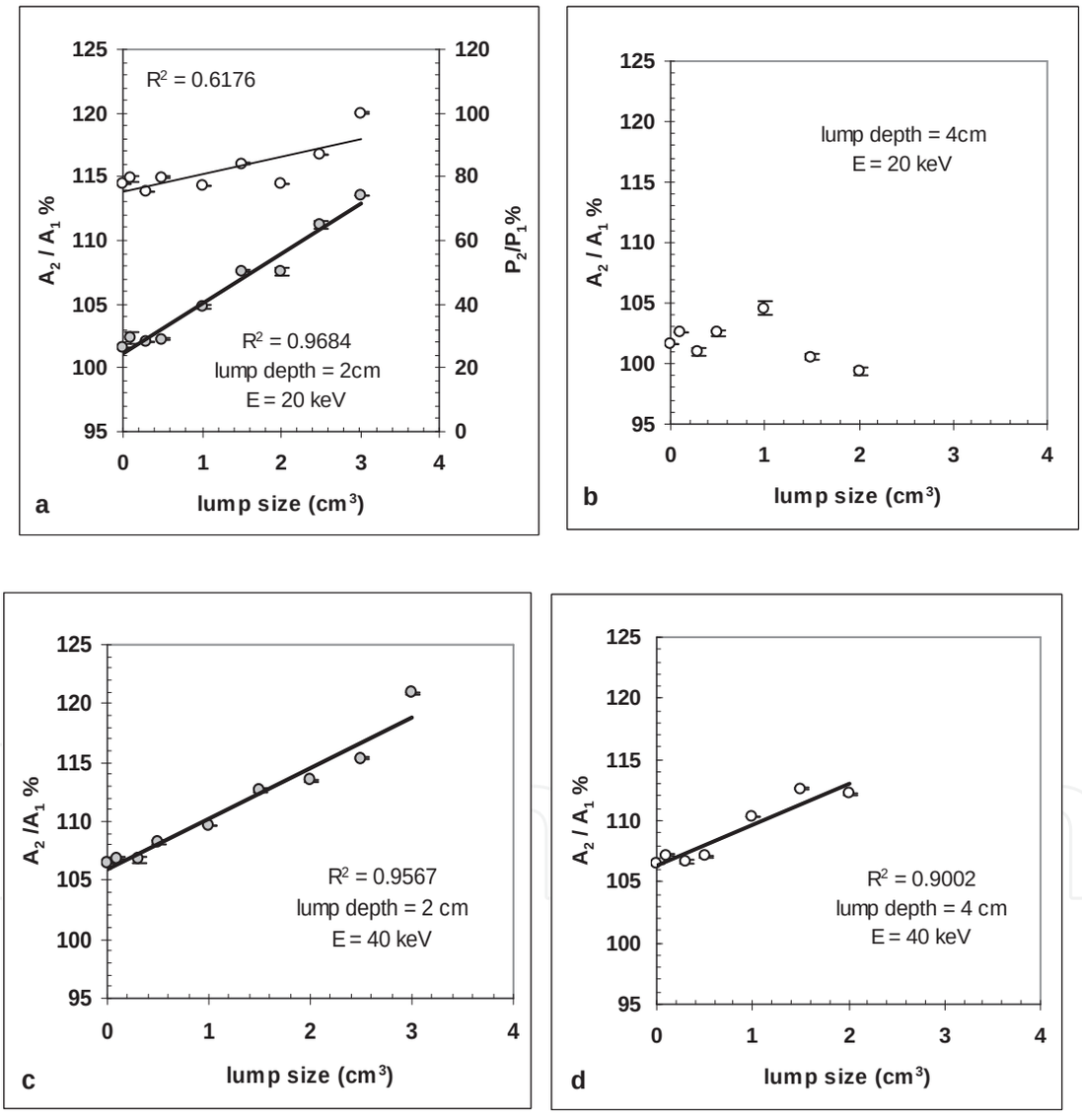


**Figure 4.** Variation of the ratio of areas ($A_2/A_1$%) under the x-ray scattering peaks at 1.6nm$^{-1}$ and 1.1 nm$^{-1}$ respectively with breast cancer lump size for 20 keV incident photons (a) lump depth 2 cm & (b) lump depth 4 cm, and for 40 keV incident photons (c) lump depth 2 cm & (d) lump depth 4 cm. Figure 4a also presents the variation of the $P_2/P_1$% ratio with lump size (right vertical axis, unfilled circles).

For breast cancer lumps located at 4cm and incident photon energy of 20keV, the variation of relative area under peak ratio ($A_2/A_1$%) with lump size produced scattered values which are far from being correlated to a linear behavior ($R^2 = 0.2006$). This result is probably due to the sharp decrease in the proportion of 20keV photons reaching the detector after interacting with the breast cancer lump located at 4cm from breast surface compared to the proportion of 20keV photons reaching the detector after interacting with the overlying tissue. This is further explained in figure 5 which shows the distribution of simulated free path lengths from the surface of the model breast of 20 and 40keV photons. While the proportion of 20 and 40keV incident photons reaching a depth of 2cm below the surface of breast are considerably high, at a depth of 4cm, the proportion of 20keV photons is substantially reduced compared to the 40keV photons reaching the same depth. This will affect the ability of characterizing the breast lump based on the distribution of scattered photons.

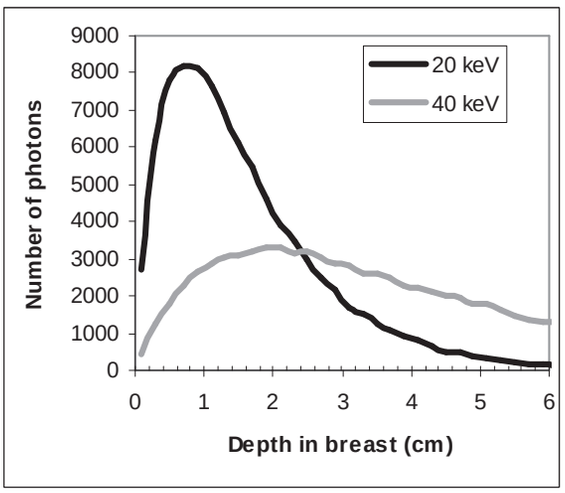


**Figure 5.** Simulated free path lengths of 20 and 40keV photons inside a model breast.

For 40keV incident photons the $A_2/A_1$% ratio varies linearly with lump depth, where the linearity and resolution of breast lumps of small sizes (up to $0.5cm^3$) is much better for breast lumps located at 2cm ($R^2 = 0.9567$) compared to that located at 4cm ($R^2 = 0.9002$) below model breast surface (figure 4c & 4d respectively).

The angular distributions of scattered photons presented in figures 2 and 3 show that for all of the investigated photon energies, lump depths and lump sizes, there exists a noticeable decrease in the total number of scattered photons with increase in lump size.

Figure 6 (a, b, c & d) presents the variation in the attenuation ($\ln I_o/I$) due to breast cancer lump measured from the total number of scattered photons in the absence ($I_o$) and in the presence (I) of breast lump of different sizes. For all of the investigated situations, there is a strong linear dependence of the $\ln I_o/I$ parameter on breast lump size. The linearity is slightly higher ($R^2 = 0.9941$ & 0.9995 for breast lumps at 2cm & 4cm depths respectively) at 40keV incident photons (figure 6 c & d) compared to the linearity ($R^2 = 0.9792$ & 0.9962 for breast lumps at 2cm & 4cm depths respectively) at 20keV incident photons (figure 6 a & b). All four

http://dx.doi.org/10.5772/52787

graphs in figure 6 show better fit to a straight line compared to the graphs in figure 4 which would be considered an advantage for the ln $I_o/I$ parameter compared to the $A_2/A_1$% parameter in the determination of lump size. Moreover, breast lumps of small sizes (up to 0.5cm$^3$) are much better differentiated using the ln $I_o/I$ parameter compared to the $A_2/A_1$% parameter (figures 6 & 4 respectively).

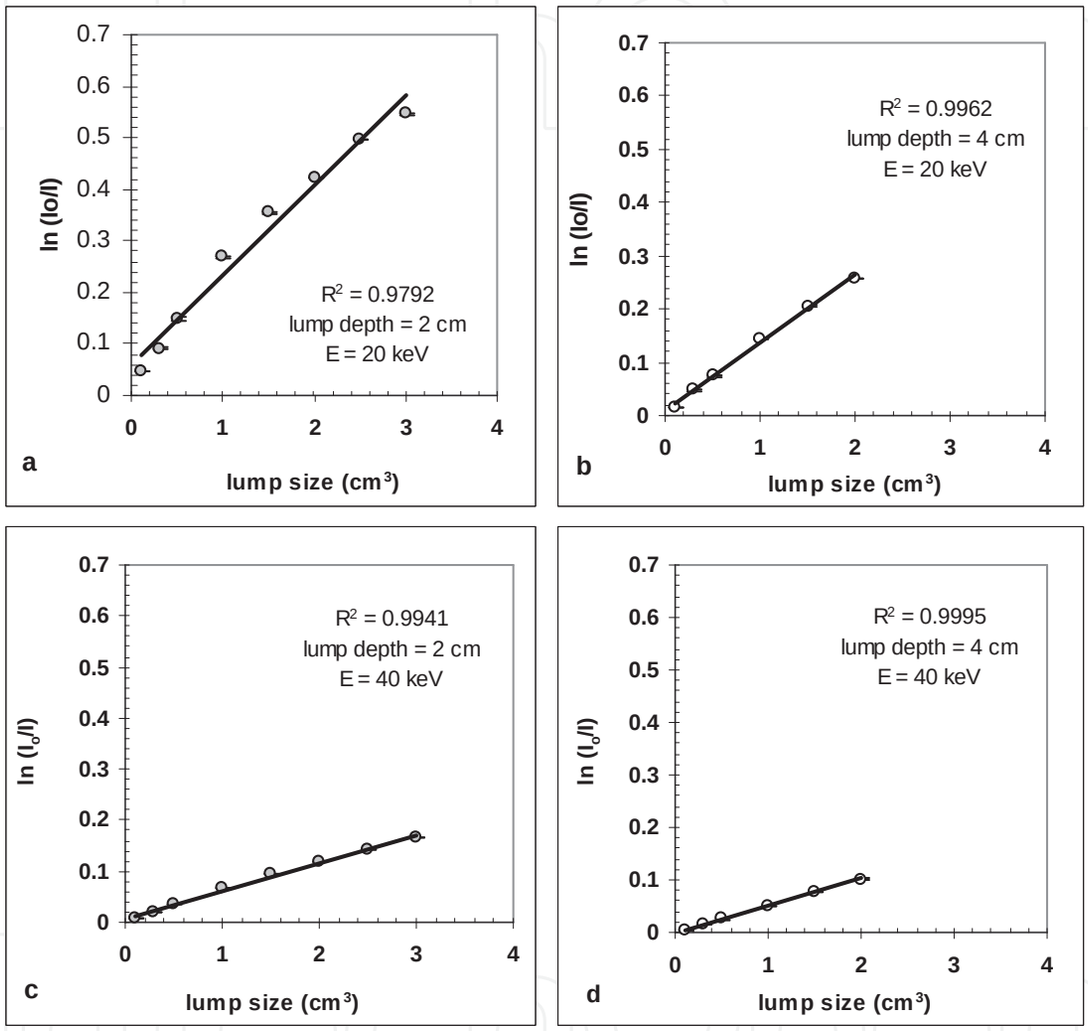


**Figure 6.** Variation of the attenuation (ln $I_o/I$) due to breast cancer lump measured from the variation in scattered photons in the absence and in the presence of breast lump of different sizes for 20keV incident photons (a) lump depth 2cm & (b) lump depth 4cm and for 40keV incident photons, (c) lump depth 2cm & (d) lump depth 4cm.

## 5. Conclusion

It has been shown that it would be possible to characterize breast cancer lumps inside a model breast of dimensions comparable to average breast dimensions using the relative difference in areas of the soft tissue to adipose peak instead of the relative intensities at a single

momentum transfer value for each peak. It has also been shown that it would be even more informative to characterize breast cancer lumps using the variation in the attenuation in scattered photons due to breast cancer lump. The data obtained at 40keV incident photon energy was always better than that obtained at 20keV. The present results show a possibility of extending the application of x-ray scattering from the detection of breast cancer in excised tissues to the detection of cancer in patients' breasts. Some possible difficulties should be overcome for applying the proposed method on patients; the availability of a monoenergetic photon source for energies between 20-40keV (a Synchrotron would be a possible solution), the design of new breast scanning system for practical testing of the present results and the development of a software specially dedicated for the analysis of acquired data and printing a user-friendly diagnostic report for the physician.

## Author details

Wael M. Elshemey

Address all correspondence to: waelelshemey@yahoo.com

Biophysics Department, Faculty of Science, Cairo University, Giza, Egypt

## References

[1] Kosanetzky J, Knoerr B, Harding G and Neitzel U 1987 X-ray diffraction measurement of some plastic materials and body tissues *Med. Phys.* 14 526–32.

[2] Kidane G, Speller R D, Royle G J and Hanby A M 1999 X-ray scatter signatures for normal and neoplastic breast tissues. *Phys. Med. Biol.* 44 1791–1802.

[3] Evans S H, Bradley D A, Dance D R, Bateman J E and Jones C H 1991. Measurement of small-angle photon scattering for some breast tissues and tissue substitute materials. *Phys. Med. Biol.*, 36, 7-18.

[4] Poletti M E, Goncalves O D and Mazzaro I 2002a Coherent and incoherent scattering of 17.44 and 6.93 kev x-ray photons scattered from biological and biological-equivalent samples: characterization of tissues. *X-Ray Spectrom*. 31, 57–61.

[5] Ryan E, and Farquharson M J 2004. Angular dispersive X-ray scattering from breast tissue using synchrotron radiation. *Radiat. Phys. Chem.* 71, 971–972.

[6] Castro C R F, Barroso R C, Anjos M J, Lopes R T, and Braz D 2004 Coherent scattering characteristics of normal and pathological breast human tissues *Radiat. Phys. Chem.* 71 649–651.

[7] Geraki K, Farquharson M, Bradley D 2004 X-ray fluorescence and energy dispersive X-ray diffraction for the characterisation of breast tissue *Radiation Physics and Chemistry* 71 969–970.

[8] Ryan Elaine A and Farquharson Michael J 2007. Breast tissue classification using x-ray scattering measurements and multivariate data analysis. *Phys. Med. Biol*. 52 6679–6696.

[9] Theodorakou C And Farquharson M J 2008 Human Soft Tissue Analysis Using X-Ray Or Gamma-Ray Techniques. *Phys. Med. Biol.* 53 R111–R149.

[10] Elshemey W M and Elsharkawy W B 2009 Monte Carlo simulation of x-ray scattering for quantitative characterization of breast cancer *Phys. Med. Biol*. 54 3773–84.

[11] Bohndiek Sarah E, Cook Emily J, Arvanitis Costas D, Olivo Alessandro, Royle Gary J, Clark Andy T, Prydderch Mark L, Turchetta Renato and Speller Robert D 2008 A CMOS active pixel sensor system for laboratorybased x-ray diffraction studies of biological tissue. *Phys. Med. Biol*. 53 655–672.

[12] Wael M Elshemey, Omar S Desouky, Mostafa M Fekry, Sahar M Talaat and Anwar A Elsayed 2010. The diagnostic capability of x-ray scattering parameters for the characterization of breast cancer, *Med. Phys* 37 4257-4265.

[13] Boone John M, Yu Tong and Seibert Anthony 1998 Mammography spectrum measurement using an x-ray diffraction device *Phys. Med. Biol.* 43 2569

[14] Ducote, Justin L. and Molloi Sabee 2010 Quantification of breast density with dual energy mammography: An experimental feasibility study *Med. Phys.* 37, 793-801.

[15] Hubbell J H 1969 Photon cross sections, attenuation coefficients, and energy absorption coefficients from 10 keV to 100 GeV *NSRDS-NBS* 29 (Washington, DC: National Bureau of Standards).

[16] Johns P C and Wismayer M P 2004 Measurement of coherent x-ray scatter form factors for amorphous materials using diffractometers *Phys. Med. Biol.* 49 5233–50

[17] Tartari Agostino, Casnati Ernesto, Bonifazzi Claudio and Baraldi Claudio 1997. Molecular differential cross sections for x-ray coherent scattering in fat and polymethyl methacrylate. *Phys. Med. Biol*. 42, 2551–2560.

[18] Tartari A, Taibi A, Bonifazzi C and Baraldi C 2002. Updating of form factor tabulations for coherent scattering of photons in tissues. *Phys. Med. Biol.* 47 163–175.

[19] Peplow Douglas E and Verghese Kuruvilla 1998. Measured molecular coherent scattering form factors of animal tissues, plastics and human breast tissue. *Phys. Med. Biol.* 43 2431–2452.

[20] Poletti M E, Goncalves O D, Schechter H, Mazzaro I 2002b Precise evaluation of elastic differential scattering cross-sections and their uncertainties in X-ray scattering experiments. *Nucl. Instrum. Methods Phys. Res. B* 187, 437–446.

[21] King B W and Johns P C 2010 An energy-dispersive technique to measure x-ray coherent scattering form factors of amorphous materials *Phys. Med. Biol.* 55 855-871

[22] Chan H P and Doi K 1986 Some properties of photon scattering in water phantoms in diagnostic radiology *Med. Phys.* 13 824–30.

[23] Elshemey Wael M, Elsayed Anwar A and El-Lakkani Ali 1999. Physical characteristics of X-ray scattering in fat and blood *Radiat. Meas*. 30 715–723.

[24] Chan H P and Doi K 1983 The validity of Monte Carlo simulation in studies of scattered radiation in diagnostic radiology *Phys. Med. Biol.* 28 109–29.

[25] Dance D. R., Skinner C. L., Carlsson G. Alm 1999 Breast dosimetry *Applied Radiation and Isotopes*, 50, 85-203

[26] Highnam R, Jeffreys M, McCormack V, Warren R, Smith G Davey and Brady M2007 comparing measurements of breast density Phys. Med. Biol. 52 5881

[27] Griffiths J A, Royle G J, Hanby A M, Horrocks J A, Bohndiek S E and Speller R D 2007 Correlation of energy dispersive diffraction signatures and microCT of small breast tissue samples with pathological analysis. *Phys. Med. Biol.* 52 6151–6164.

[28] Hubbell J H, Veigele Wm J, Briggs E A, Brown R T, Cromer D T and Howerton R J 1975 Atomic form factors, incoherent scattering functions and photon scattering cross-sections *J. Phys. Chem. Ref. Data* 4 471–538.

[29] Hubbell J H 1977 Photon mass attenuation and mass energy-absorption coefficients for H, C, N, O, Ar and seven mixtures from 0.1 keV to 20 MeV *Radiat. Res.* 70 58–81.